Modeling of III-Nitride Quantum Wells with Arbitrary Crystallographic Orientation for Nitride-Based Photonics

Mikhail V. Kisin*, Robert Brown and Hussein S. El-Ghoroury
Ostendo Technologies, Inc.
*Corresponding author: 6185 Paseo del Norte, Ste. 200, Carlsbad, CA 92011 (mikhail@ostendo.com)

Abstract: A program for self-consistent modeling of electron-hole energy spectrum and space-charge distribution in III-nitride based quantum well (QW) structures has been developed. The program assumes arbitrary crystallographic orientation of the heterostructure template. The model takes into consideration full 6-band description of the valence band states, nonparabolicity of the electron spectrum, quantum confinement of electrons and holes, strain induced modifications of the band structure, spontaneous- and piezo-polarization fields, background layer doping, and variable level of charge carrier injection. Calculated optical characteristics include electron-hole optical susceptibility, spontaneous and stimulated emission rates, polarization coefficients for light emission and absorption, radiative recombination rates, and optical gain spectra in optically active nitride QWs.

Keywords: III-Nitride semiconductors, nonpolar and semipolar structures, light emitting diodes, laser diodes, photonics.

1. Introduction

Applications of nitride-based photonic devices in visible and UV optical ranges are growing rapidly. The most commonly used heterostructures for such applications include a sequence of GaInN quantum wells grown on a polar substrate plane (crystallographic hexagonal *c*-plane). Even in this symmetric configuration, the quantum mechanical description of the QW electronic properties and subsequent modeling of the QW optical characteristics is very complicated if compared to more traditional III-V semiconductor materials with highly symmetric cubic crystal lattice. III-Nitride structures grown on nonpolar and semipolar substrates with less symmetric crystallographic planes (*m*-type and *a*-type planes) are much more favorable for optoelectronic devices due to the lower piezo-polarization fields and, possibly, higher level of indium incorporation in the QW composite material. Correspondingly, the modeling complexities grow.

2. The Model

To provide an adequate tool for modeling the nitride-based devices with nonpolar/semipolar growth planes the multiband matrix Hamiltonian established for semiconductors with hexagonal symmetry has been transformed to an inclined coordinate system related to the growth plane of the reduced symmetry. The resulting system of six equations for valence band states (holes), an effective-mass Schrodinger equation for conduction band states (electrons), and Poisson equation for the confined carriers has been solved iteratively for an arbitrary level of injected carrier concentration. The strain tensor components calculated in the inclined coordinate system affect the solution and eigenstates both through the deformation potential terms in the Hamiltonian and by contributing to the induced piezo-polarization charges at the QW boundaries.

3. The Modeling

The general structure of the developed software is analogous to previously reported programs for mid-infrared QW lasers based on cubic semiconductors [1]. Due to inadequate capabilities of COMSOL GUI for quantum mechanical calculations, most of the modeling was performed directly in COMSOL. A one-dimensional eigenvalue solver for quantum mechanical equations and a stationary solver for Poisson equation have been used iteratively revealing good conversion rate (5-15 iterations per step-like increase in the injected carrier concentration). Special subprograms were developed for orthogonalization of the degenerate valence band eigenstates, QW subband dispersion analysis, modeling of the temperature-induced carrier redistribution between the QW subbands, and calculation of the structure optical characteristics.

Program input includes band structure parameters of binary nitride compounds and bowing parameters for the interpolation scheme, elastic, piezoelectric and dielectric constants, structure layout, electrical bias and ambient conditions.

The modeling provides the following information: conduction and valence band profiles including spontaneous polarization, piezo-polarization and self-consistent Coulomb field due to the charge redistribution in QWs, strain and deformation tensor components, confined energy levels and subband dispersions, electron and hole subband density of states functions, carrier distribution functions and subband populations at arbitrary level of injection, matrix elements and anisotropy coefficients for optical transitions, spontaneous and stimulated emission spectra, effective radiative recombination rate, QW optical gain spectra and carrier-induced refractive index change, differential and peak optical gain coefficients, temperature and injection dependencies of the calculated characteristics.

4. Illustrative results

Figure 1 shows the conduction (upper plots) and valence (lower plots) band profiles in an exemplary $GaN/Ga_{0.8}In_{0.2}N/GaN$ QW structure grown in different crystallographic orientations: polar (00.1), semipolar (11.2), and nonpolar (11.0). For all the structures the QW width was 2 nm and self-consistent calculations were performed at the carrier injection level corresponding to the QW transparency point. Intra-QW screening of internal fields is weak at this level of injection. In polar QW, the band tilting due to the strain-induced piezoelectric field results in strong spatial carrier separation.

Figure 2 shows valence band subband dispersions in nominally the same structures grown in different crystallographic orientations, including *a*-type and *m*-type plane families. The calculations reveal close similarity between semipolar and nonpolar structures and demonstrate noticeable strain-induced increase of the energy separation between the two upper hole subbands in *a*-type and *m*-type structures comparing to the much smaller subband separation in polar *c*-plane structure. The energy reference level ($E = 0$) for valence band states in this plot corresponds to the uppermost bulk valence band level at the center point of the QW. This visualizes the quantum confinement and band tilting effects in the QW valence band. The Y-direction of the coordinate system corresponds to the projection of the *c*-axis on the growth plane in semipolar/nonpolar structures, with Z-axis being the structure growth direction.

Figure 3 compares the QW material gain spectra in structures with polar, semipolar, and nonpolar orientations. For each orientation, the subplots show the gain evolution with the increasing QW width. In the nonpolar structure, the red shift of the gain spectrum is related to the decrease of the carrier confinement energy, while the decline of the peak gain should be attributed to the decrease in the hole subband separation; see Figure 4 for subband dispersion evolution. The latter trend leads to thermal hole redistribution at elevated temperatures and correspondingly degrades the optical gain. In semipolar and, especially, in polar structures, the gain deterioration is also affected by the decreasing wave function overlap in wider QWs; see Figure 5 which shows spatial redistribution of the electron and hole states in the semipolar (11.2) structure with increasing QW width. QW indium concentration is 30% and the injection level corresponds to the QW transparency point. Weak screening of the piezoelectric field by the injected carriers is noticeable in the wider QWs.

Figure 6 shows red shift of the QW optical gain spectra in QWs with increasing indium concentration. This shift is determined by strong dependence of the GaInN band gap on the Indium contents. Figure 7 illustrates the temperature-induced red shift of the optical spectra due to the band gap temperature dependence. In Figure 7, the spontaneous emission rate is compared with the stimulated emission rate per one photon in the cavity. Light with Y-polarization, depressed in the gain spectra, is fully represented in the spontaneous emission. Low value of the optical broadening (1 meV) was adopted for this calculation to resolve the spectral features. Spectral integration of the spontaneous emission rates defines the value of the QW effective radiative recombination coefficient B, which includes the effect of electron-hole spatial separation. At temperature 75C the corresponding values of B coefficient were obtained as (0.0045, 0.66, and 0.83)$\times 10^{-10}$ cm^3/s for polar, semipolar and nonpolar QW structures respectively.

5. Conclusions

The described program will be used at Ostendo Technologies Inc. as a core for a full-scale modeling of III-nitride based optoelectronic devices with arbitrary crystallographic orientation of the substrate template.

6. References

1. M.V. Kisin, “Modeling of the Quantum Well and Cascade Semiconductor Lasers using 8-Band Schrödinger and Poisson Equation System”, Proceedings of COMSOL Conference, Oct. 4-6, 2007, Newton, MA, USA. pp. 489-493.

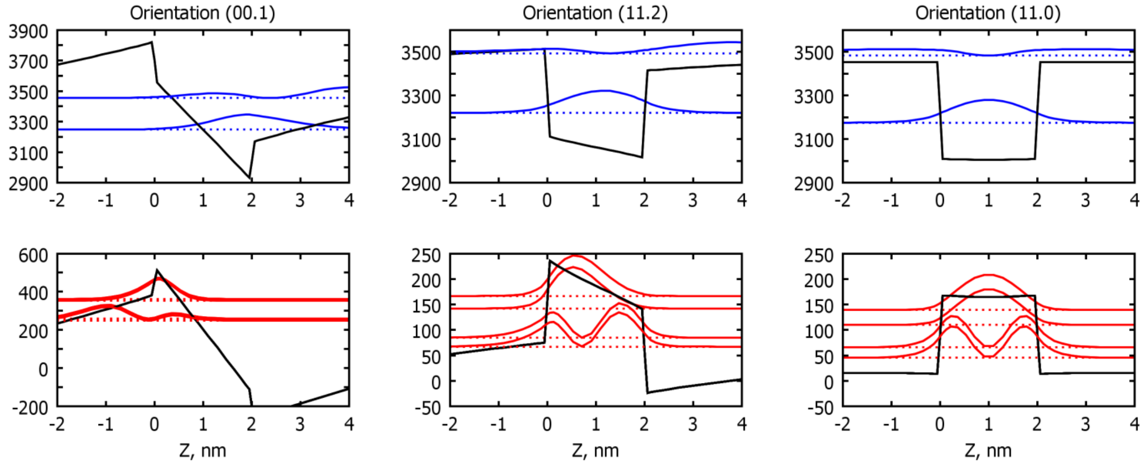

Figure 1. Conduction and valence band profiles in III-nitride QWs with different crystallographic orientations. QW indium concentration is 20%. T = 300K.

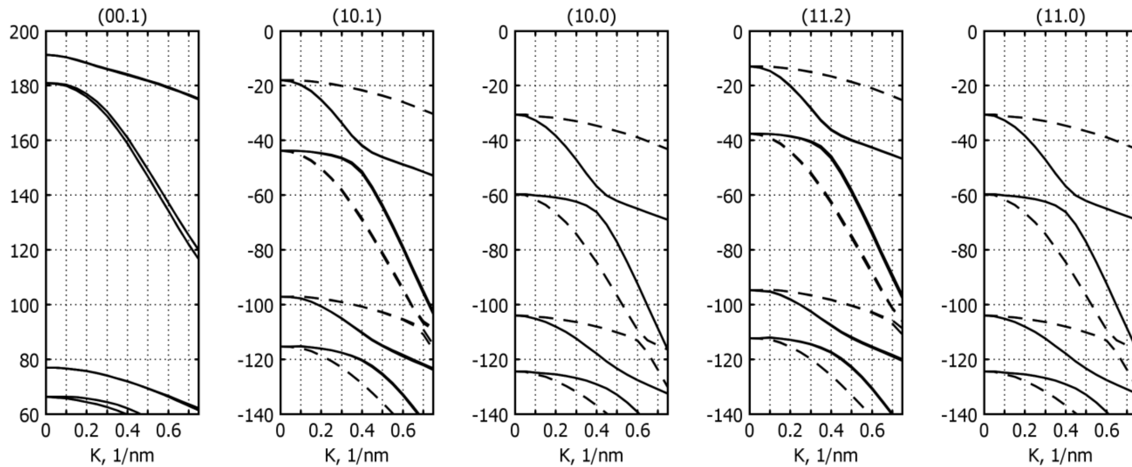

Figure 2. Conduction and valence band profiles in QWs with different crystallographic orientations: polar (00.1), semipolar (10.1) and (11.2), and nonpolar (10.0) and (11.0). Solid and dashed lines represent hole dispersions along K_x and K_y directions. QW indium concentration is 20%. T = 300K.

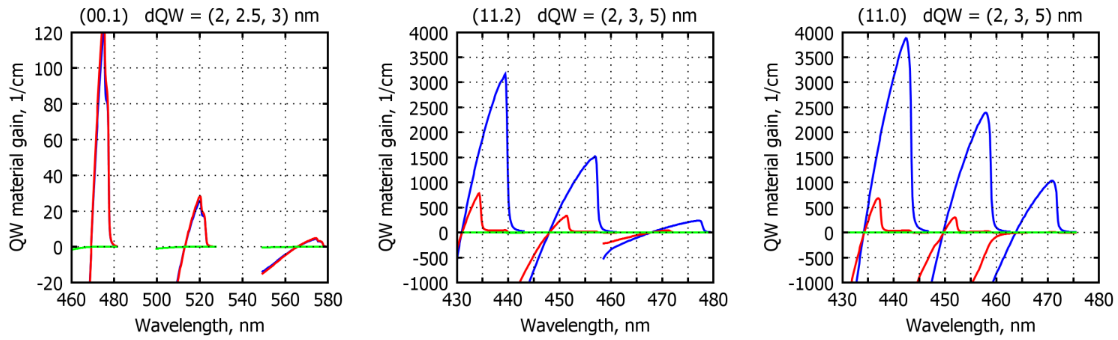

Figure 3. Gain spectra modification with increasing QW width in polar, semipolar, and nonpolar QW structures. Optical field polarization: blue – X, red – Y. QW indium concentration is 30%. Carrier injection level is $5x10^{12}$ cm^{-2}. T = 300K.

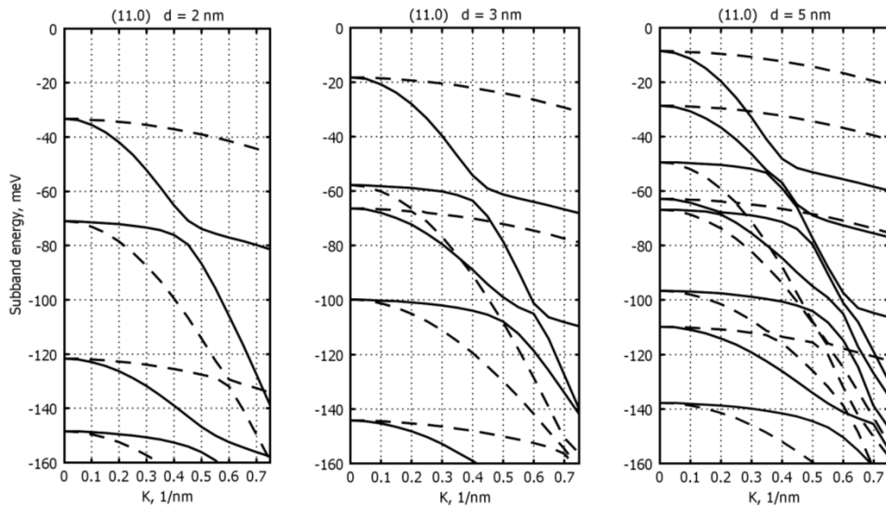

Figure 4. Evolution of the valence subband dispersions with increasing QW width in nonpolar (11.0) QW structure with 30% indium and transparency point injection level.

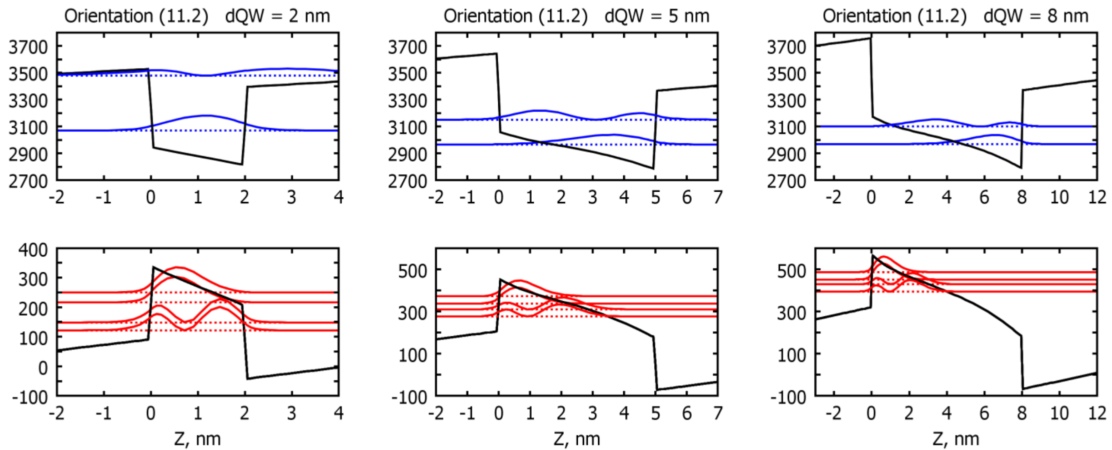

Figure 5. Spatial redistribution of the electron and hole states in semipolar (11.2) QW.

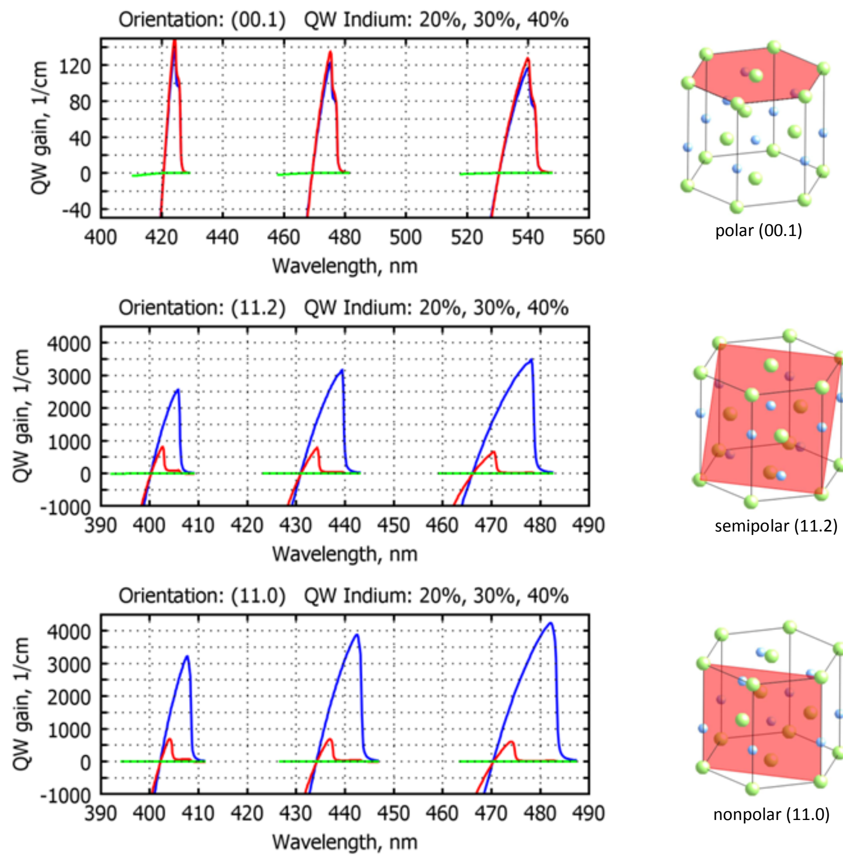

Figure 6. Red shift of the QW material gain spectra with increasing QW indium concentration for different crystallographic orientations. QW width is 2 nm. T = 300K. Injection level $5x10^{12}$ cm^{-2}. Blue (red) lines – X (Y) polarization of the optical field.

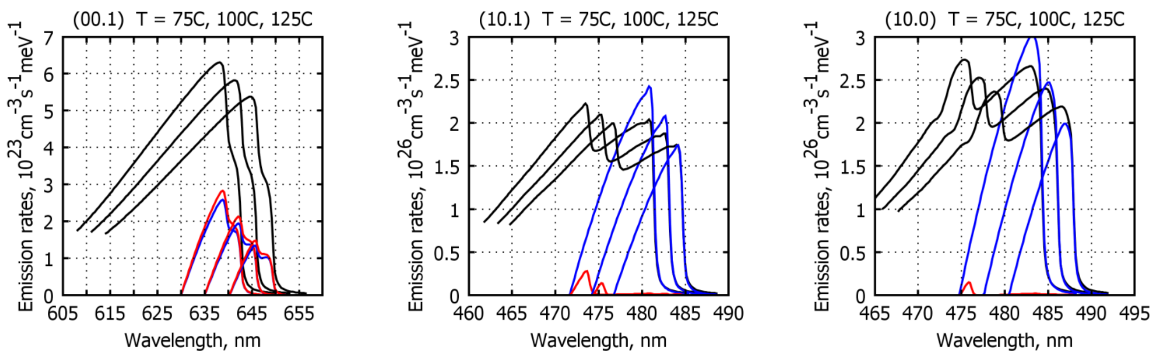

Figure 7. Comparison of spontaneous emission rates (black lines) and stimulated emission rates (colored) per single photon in cavity. Blue and red curves show stimulated emission rates for X and Y polarization of the optical field. QW indium concentration is 35%. QW width is 3 nm. Injected carrier concentration is $5x10^{12}$ cm^{-2}.